Theoretical analysis of the EAST 4-strap ion cyclotron range of frequency antenna with variational theory

You may also be interested in:

Analysis of the coupling properties of the toroidal antenna array in JFT-2M by a code considering the solid septa
M. Saigusa, T. Yamamoto, C.C. Petty et al.

An ICRF antenna for the next step tokamak operating in a wide frequency band
V.P. Bhatnagar and J. Jacquinot

High coupling performance of JT-60U ICRF antennas
M. Saigusa, S. Moriyama, T. Fujii et al.

Recent developments in ICRF antenna modelling
P.U. Lamalle, A.M. Messiaen, P. Dumortier et al.

Variational theory of the ICRH antenna
K. Theilhaber and J. Jacquinot

Antenna optimization for Alfvén wave heating
S. Puri

Simulation of parasitic edge ion Bernstein wave coupling during fast wave heating
M.H. Bettenhausen and J.E. Scharer

Theory of the JET ICRH antenna
K. Theilhaber

Mechanical Design and First Engineering Commissioning of ICRF Antenna for EAST
Yang Qingxi, Song Yuntao, Wu Songtao et al.

Theoretical analysis of the EAST 4-strap ion cyclotron range of frequency antenna with variational theory[*]

Jia-Hui Zhang(张珈珲)[1,2], Xin-Jun Zhang(张新军)[1,†], Yan-Ping Zhao(赵燕平)[1],

Cheng-Ming Qin(秦成明)[1,‡], Zhao Chen(陈照)[1,2], Lei Yang(杨磊)[1,2], and Jian-Hua Wang(王健华)[1]

[1] *Institute of Plasma Physics, Chinese Academy of Sciences, Hefei 230031, China*
[2] *University of Science and Technology of China, Hefei 230026, China*

A variational principle code which can calculate self-consistently currents on the conductors is used to assess the coupling characteristic of the EAST 4-strap ion cyclotron range of frequency (ICRF) antenna. Taking into account two layers of antenna conductors without lateral frame but with slab geometry, the antenna impedances as a function of frequency and the structure of RF field excited inside the plasma in various phasing cases are discussed in this paper.

1. Introduction

Heating in the ion cyclotron range of frequencies (ICRF) is one of the important auxiliary heating methods in the EAST tokamaks. A key issue is the improvement of the coupling between the ICRF antenna and the plasma. Over the past years, a lot of efforts have been made to analyze and design the ICRF antenna.[1–4] In this paper, we will apply a variational theory to evaluate the coupling characteristic of the EAST 4-strap ICRF antenna.

Theihaber and Jacquinot came up with the variational theory to calculate the self-consistent current distribution in the straps of the simple back-to-back ICRF antenna[5] and then improved the coupling code to take into account a more complicated trombone antenna geometry surrounded by an opaque frame[6] in JET. The coupling code was extended by Saigusa et al. so that it can be applied to a toroidal trombone antenna array with solid septa[7] despite its complication. Zhang *et al.* made some progress on Theihaber and Jacquinot's coupling code to analyze the ICRF antenna array in HT-7U.[8] In the present paper, the EAST 4-Strap ICRF antenna impedances as a function of frequency and the structure of RF field excited inside the plasma in various phasing cases are presented by using a modification coupling code with the variational theory. For simplicity, the naked ICRF antenna model without lateral structure is employed in spite of the effect produced by the limiter frame while multiple current conductors are taken into account. The rest of this paper is organized as follows. In Section 2 the 4-strap ICRF antenna model is described, and the derivation of the wave equations in vacuum is also

re-presented. In Section 3, we investigate the variation of the input impedance at the feeder point relating to antenna parameters and compare the RF field structures in different antenna phasing cases. Conclusions about the 4-strap ICRF antenna model are drawn in Section 4.

2. Model and variational theory

2.1. Description of the model

The model of a single antenna is shown in Fig. 1. The z direction of the coordinate is parallel to toroidal magnetic field B_T, the y direction is in the poloidal field direction, and the x direction is in the radial direction pointing to the plasma. The antenna conductors are represented by infinitely thin metallic sheets. They radiate through an ideal electrostatic screen, which is perfectly conducting in the z direction and perfectly insulating in the y direction. This screen is completely opaque to the TM modes ($E_z \neq 0$) and completely transparent to the TE modes ($H_z \neq 0$), which carry the power into the plasma.
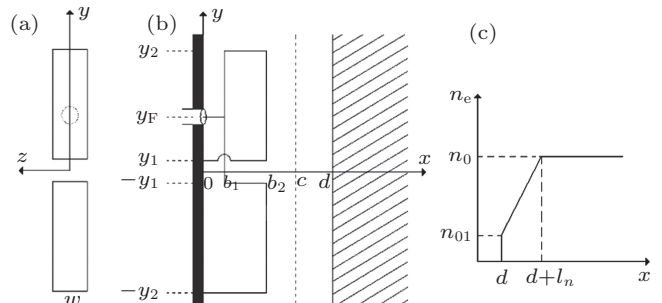

Fig. 1. Geometry of the coupling model: (a) schematic view, (b) poloidal cross-sectional view for the single ICRF antenna, and (c) plasma density profile.

http://iopscience.iop.org/cpb   http://cpb.iphy.ac.cn

Table 1. Antenna parameters.

Parameters/m		Parameters/m	
y_1	0.01	b_1	0.02
y_2	0.4	b_2	0.12
$y_F = (y_2 - y_1)/2$	0.195	c	0.13
w	0.1	d	0.14

The back wall of the antenna is located at $x = 0$, the electrostatic screen at $x = c$ and the plasma edge at $x = d$. The antenna consists of two main radiating conductors at $x = b_2$ and two return conductors at $x = b_1$. The feeder point connects to the return conductors at $y = y_F$. The upper main radiating conductor short point is placed at $y = y_1$ and the lower main radiating conductor short point is placed at $y = -y_2$. The widths of the conductors in the z direction are both w.

The plasma is assumed to have a linear density profile over a length l_n from a low edge density of n_{01} at $x = d$ to a maximum density of n_0 at $x = d + l_n$. The radiation condition is imposed at $x = d + l_n$ so that all outgoing waves inside the plasma are absorbed without reflection.

2.2. Derivation of the wave equations

We normalize Maxwell's equations in the calculations as done in Ref. [5]. The subscript 'p' denotes the physical quantity, then: $\boldsymbol{x} = (\omega/c)\boldsymbol{x}_P$, $\boldsymbol{E} = \boldsymbol{E}_P$, $\boldsymbol{H} = (\mu_0/\varepsilon_0)^{1/2}\boldsymbol{H}_P$, and $\boldsymbol{J} = (1/\omega\varepsilon_0)\boldsymbol{J}_P$. With these normalizations, expressions for the impedance should be multiplied by $(\mu_0/\varepsilon_0)^{1/2} = 377\ \Omega$ to recover the physical result. We then have Maxwell's equations:

$$\nabla \times \boldsymbol{E} = \mathrm{i}\boldsymbol{H}, \tag{1}$$

$$\nabla \times \boldsymbol{H} = \boldsymbol{J} - \mathrm{i}\boldsymbol{E}. \tag{2}$$

From Maxwell's equations, the equations for E_z and H_z are

$$\frac{\mathrm{d}^2 E_z}{\mathrm{d}x^2} - \Gamma^2 E_z = n_z\left(\mathrm{i}n_y J_y + \frac{\mathrm{d}J_x}{\mathrm{d}x}\right), \tag{3}$$

$$\frac{\mathrm{d}^2 H_z}{\mathrm{d}x^2} - \Gamma^2 H_z = -\frac{\mathrm{d}J_y}{\mathrm{d}x} + \mathrm{i}n_y J_x, \tag{4}$$

where

$$\Gamma^2 = n_y^2 + n_z^2 - 1. \tag{5}$$

The current distributions on conductors of the antenna are modeled by

$$J_y(x,y,z) = J_{y1}(y,z)\delta(x - b_1) + J_{y2}(y,z)\delta(x - b_2), \tag{6}$$

$$J_x(x,y,z) = J_{x1}(y,z)\gamma(b_1 - x) + J_{x2}(y,z)$$
$$\times [\gamma(b_2 - x) - \gamma(b_1 - x)] + J_{x3}(y,z)\gamma(b_2 - x), \tag{7}$$

where $\gamma(x)$ is the step-function and $\delta(x)$ the Dirac delta. The solution for E_z ($0 \le x \le c$) consistent with the boundary conditions ($E_z(x = 0) = E_z(x = c) = 0$) is:

$$E_z(x) = S(x, b_1)n_z\left[\mathrm{i}n_y J_{y1} - (J_{x1} - J_{x2})\right]$$
$$+ S(x, b_2)n_z\left[\mathrm{i}n_y J_{y2} - (J_{x2} + J_{x3})\right], \tag{8}$$

where

$$S(x, \xi) = \begin{cases} \dfrac{-\sinh[\Gamma(c - x)]\sinh(\Gamma\xi)}{\Gamma\sinh(\Gamma c)}, & x \ge \xi \ge 0, \\[3mm] \dfrac{-\sinh[\Gamma(c - \xi)]\sinh(\Gamma x)}{\Gamma\sinh(\Gamma c)}, & \xi \ge x \ge 0. \end{cases} \tag{9}$$

The boundary conditions for H_z are imposed as follows:

$$\frac{\mathrm{d}H_z(0)}{\mathrm{d}x} = 0, \tag{10}$$

$$H_z(d) = Y_P(n_y, n_z)\left(-\frac{\mathrm{i}}{1 - n_z^2}\right)\frac{\mathrm{d}H_z(d)}{\mathrm{d}x}, \tag{11}$$

where Y_P is the plasma admittance defined as

$$Y_P(n_y, n_z) = \frac{1}{Z_P(n_y, n_z)} = \frac{H_z(n_y, n_z)}{E_z(n_y, n_z)}$$

at $x = d$. The solution for H_z satisfying the boundary conditions can be written as

$$H_z(x) = T(x, b_1)\left[J_{y1} + \frac{\mathrm{i}n_y(J_{x1} - J_{x2})}{\Gamma^2}\right]$$
$$+ T(x, b_2)\left[J_{y2} + \frac{\mathrm{i}n_y(J_{x2} + J_{x3})}{\Gamma^2}\right] - \frac{\mathrm{i}n_y J_x(x)}{\Gamma^2}, \tag{12}$$

where

$$T(x, \xi) = \begin{cases} \dfrac{-\Gamma\cosh[\Gamma(d - x)] - \rho\sinh[\Gamma(d - x)]}{\Gamma\sinh(\Gamma d) + \rho\cosh(\Gamma d)}\sinh(\Gamma\xi), & x \ge \xi \ge 0, \\[3mm] \dfrac{\Gamma\sinh[\Gamma(d - \xi)] + \rho\cosh[\Gamma(d - \xi)]}{\Gamma\sinh(\Gamma d) + \rho\cosh(\Gamma d)}\cosh(\Gamma x), & \xi \ge x \ge 0, \end{cases} \tag{13}$$

and

$$\rho = \mathrm{i}\left(n_z^2 - 1\right)Z_P(n_y, n_z). \tag{14}$$

Having obtained the solutions for E_z and H_z, we can proceed

to find the other field components through the procedures in Appendix A of Ref. [5] as follows:

$$E_y = \frac{1}{1 - n_z^2}\left[-n_y n_z E_z - \mathrm{i}\frac{\mathrm{d}H_z}{\mathrm{d}x}\right], \tag{15}$$

$$E_x = \frac{1}{1-n_z^2}\left[\mathrm{i}n_z\frac{\mathrm{d}E_z}{\mathrm{d}x} - n_y H_z\right] - \frac{\mathrm{i}}{1-n_z^2}[J_x], \quad (16)$$

$$H_y = \frac{1}{1-n_z^2}\left[-n_y n_z H_z + \mathrm{i}\frac{\mathrm{d}E_z}{\mathrm{d}x}\right], \quad (17)$$

$$H_x = \frac{1}{1-n_z^2}\left[\mathrm{i}n_z\frac{\mathrm{d}H_z}{\mathrm{d}x} + n_y E_z\right]. \quad (18)$$

Furthermore, the feeder point impedance can be written in the variational form as

$$Z_A = \frac{\int_D \boldsymbol{K}\cdot\boldsymbol{E}(\boldsymbol{J})\,\mathrm{d}\boldsymbol{R}}{I_{AK}I_{AJ}}. \quad (19)$$

We can calculate the integration by using Parseval's theorem

$$
\int_D \boldsymbol{K}\cdot\boldsymbol{E}(\boldsymbol{J})\,\mathrm{d}\boldsymbol{R}
$$
$$
= \sum_{\substack{\alpha_1,\alpha_2=x,y \\ \beta_1,\beta_2=1,2,3}} \iint \frac{\mathrm{d}n_y}{2\pi}\frac{\mathrm{d}n_z}{2\pi} K_{\alpha_2\beta_2}(-n_y,-n_z)
$$
$$
\times R_{\alpha_2\beta_2,\alpha_1\beta_1}(n_y,n_z)J_{\alpha_1\beta_1}(n_y,n_z). \quad (20)
$$

In Eqs. (19) and (20), D denotes the surface of the central conductors, $\boldsymbol{J}$ and $\boldsymbol{K}$ are trial functions for the currents, and I_{AJ} and I_{AK} are the total currents flowing at the feeder point, which are consistent with $\boldsymbol{J}$ and $\boldsymbol{K}$, respectively.

The condition $\delta Z_A = 0$ will lead to the physical current $\boldsymbol{J}$ flowing in the conductors and the corresponding antenna impedance Z_A at the feeder point.

2.3. Choice of trial functions for a single strap antenna

For simplicity, we assume that the current on the conductor in the z direction is uniform because the conductors are much longer than width, and the width is much shorter than a wavelength at the operating frequency. Then

$$\boldsymbol{J}(y,z) = \boldsymbol{J}(y)M(z), \quad (21)$$

where $M(z) = 1$ on the conductor ($|z| \le w/2$) and is 0 otherwise.

In order to satisfy continuity conditions at the connections and the short-circuit condition $\mathrm{d}J_{y2}(y)/\mathrm{d}y = 0$ at $y = y_1$ and $y = -y_2$, we take advantage of the current distributions corresponding to the transmission line model in the upper and lower conductors, respectively. The upper and the lower antenna loop are balanced ($y_F = (-y_1+y_2)/2$), so we can write down the trial functions as follows:

$$J_{y1}^{(n)}(y) = \cos[nk(-y+|2y_2-y_1|)][\gamma(y-y_F)-\gamma(y-y_2)]$$
$$- \cos[nk(y+y_2)][\gamma(y-y_1)-\gamma(y-y_F)], \quad (22)$$

$$J_{y2}^{(n)}(y) = -\cos[nk(y-y_1)][\gamma(y-y_1)-\gamma(y-y_2)]$$
$$- \cos[nk(y+y_2)][\gamma(y+y_2)-\gamma(y+y_1)], \quad (23)$$

$$J_{x1}^{(n)}(y) = 2\cos[nk(y_F+y_2)]\delta(y-y_F), \quad (24)$$

$$J_{x2}^{(n)}(y) = \cos[nk(y_2-y_1)]\delta(y-y_2)$$

$$+ \cos[nk(y_2-y_1)]\delta(y+y_1), \quad (25)$$

$$J_{x3}^{(n)}(y) = -\delta(y-y_1)-\delta(y+y_2), \quad (26)$$

where $\gamma(x)$ is the step-function $\gamma(x) = 0$, $1/2$, 1 for $x < 0$, $x = 0$, $x > 0$, respectively. We could express each current in terms of a linear combination of these trial functions:

$$J_{\alpha_1\beta_1}(y,z) = \sum_{n=0}^{N} a_n J_{\alpha_1\beta_1}^{(n)}(y)M(z), \quad (27)$$

$$K_{\alpha_2\beta_2}(y,z) = \sum_{n=0}^{N} b_n J_{\alpha_2\beta_2}^{(n)}(y)M(z). \quad (28)$$

Here, a_n and b_n are the coefficients for $\boldsymbol{J}$ and $\boldsymbol{K}$, where $n = 0$, 1, ..., N. $N = 4$–5 is large enough to result in a rather small calculation error for Z_A. With these trial functions, equation (19) can be rewritten as

$$Z_A = \frac{\sum_{m,n} b_m L_{mn} a_n}{\left(\sum_n a_n P_n\right)\left(\sum_m b_m P_m\right)}, \quad (29)$$

where $P_n = 2w\cos[nk(y_F+y_2)]$ and the matrix elements are as follows:

$$L_{mn} = \sum_{\substack{\alpha_1,\alpha_2=x,y \\ \beta_1,\beta_2=1,2,3}} \iint \frac{\mathrm{d}n_y}{2\pi}\frac{\mathrm{d}n_z}{2\pi} K_{\alpha_2\beta_2}^{(m)}(-n_y,-n_z)$$
$$\times R_{\alpha_2\beta_2,\alpha_1\beta_1}(n_y,n_z)J_{\alpha_1\beta_1}^{(n)}(n_y,n_z). \quad (30)$$

Requiring an extremum $\delta Z_A = 0$, we will obtain an input impedance at the feeder point and the physical current coefficients on conductors:

$$Z_A = \frac{1}{\boldsymbol{P}\cdot\boldsymbol{L}^{-1}\cdot\boldsymbol{P}}, \quad (31)$$

$$\boldsymbol{a} = Z_A\left(\boldsymbol{L}^{-1}\cdot\boldsymbol{P}\right), \quad (32)$$

$$\boldsymbol{b} = Z_A\left(\boldsymbol{P}\cdot\boldsymbol{L}^{-1}\right), \quad (33)$$

where $\boldsymbol{L} = \|L_{mn}\|$ and $\boldsymbol{P} = (P_0\cdots P_N)^{\mathrm{T}}$.

2.4. Extension for the antenna array

The situation with four identical current straps in the z direction can be treated by rewriting the current distribution and resolving Maxwell's equations. The current distribution for the N-strap antenna array can be written as

$$\boldsymbol{J}_{\mathrm{array}} = \sum_{n=0}^{N-1} \boldsymbol{J}(x,y,z-n\cdot\Delta z)\cdot\exp(\mathrm{i}\varphi_n), \quad (34)$$

where $\boldsymbol{J}(x,y,z)$ is the current distribution for a single strap antenna, Δz is the period of the antenna array in the z direction, and φ_n is the current phase of the n-th current strap. If the mutual coupling between current straps is ignored, we can obtain the impedance for each current strap by modifying Eq. (19) into the following expression:

$$Z_A = \frac{1}{N}\frac{\int_D \boldsymbol{K}\cdot\boldsymbol{E}(\boldsymbol{J}_{\mathrm{array}})\,\mathrm{d}\boldsymbol{R}}{I_{AK}I_{AJ}}. \quad (35)$$

3. Simulation results

In this section, first we give the frequency scans in the presence of the plasma for a single ICRF antenna. Then, we investigate the antenna behavior dependent on the antenna parameters at 30 MHz around which the EAST ICRF antenna operates frequently. Finally, the field structures corresponding to the single ICRF antenna and the ICRF antenna array are provided.

3.1. Frequency characteristics

Frequency scans with and without the plasma for a single strap ICRF antenna are shown in Fig. 2. The antenna parameters are listed in Table 1. The plasma edge density is assumed to be $n_{01} = 3 \times 10^{12}$ cm^{-3}, the central density $n_0 = 2 \times 10^{13}$ cm^{-3}, and the linear profile length $l_n = 0.1$ m. In the following figures, the line with black squares represents the resistance of the impedance $R = \mathrm{Re}(Z_A)$ and the line with white squares refers to the reactance $X = \mathrm{Im}(Z_A)$. According to the definition of the code, the negative and the positive signs of X represent the inductive and capacitive reactances, respectively. Figure 2(a) shows that the single strap ICRF antenna in vacuum becomes resonant at $f = 31$ MHz, where R reaches a maximum value and X starts to approach to zero rapidly. The minor peak of R occurs at $f = 28$ MHz because of the larger numerical calculation error near the resonant point.
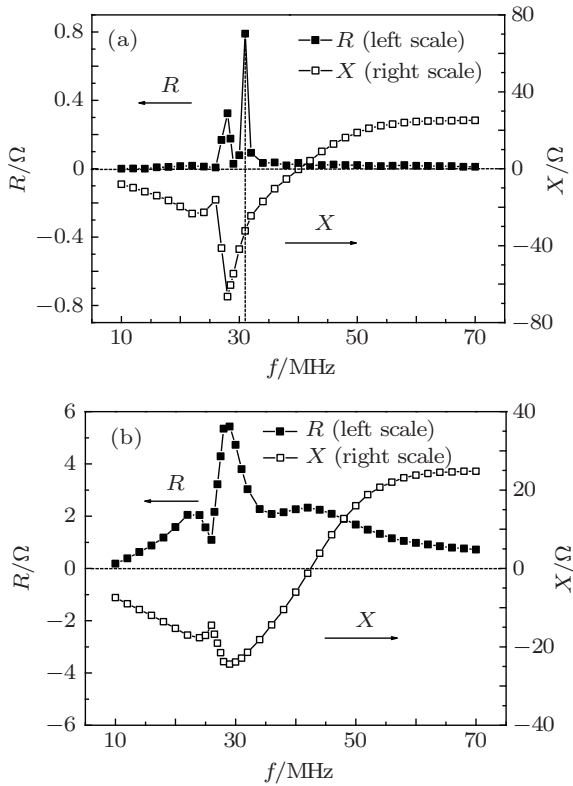
Fig. 2. (a) Frequency scans of the antenna impedance $Z_A = R + iX$ in vacuum. The line with black squares represents the resistance of the impedance $R = \mathrm{Re}(Z_A)$ and the line with white squares refers to the reactance $X = \mathrm{Im}(Z_A)$. (b) Frequency scans of the antenna impedance $Z_A = R + iX$ in the presence of a DH plasma: $n_\mathrm{D}/n_\mathrm{e} = 0.9$, $n_\mathrm{H}/n_\mathrm{e} = 0.1$, $B = 2.3$ T, $n_{01} = 3 \times 10^{12}$ cm^{-3}, $n_0 = 2 \times 10^{13}$ cm^{-3}, $l_n = 0.1$ m, the antenna parameters are indicated in Table 1.

As shown in Fig. 2(b), the presence of the plasma smooths the frequency responses of R and X in vacuum. R is much larger and inductive reactance is smaller than their counterparts of vacuum condition in Fig. 2(a).

3.2. Dependence on antenna parameters

Figure 3 shows the variations of real part (resistance) and imaginary part (reactance) of impedance with antenna parameters for a single antenna. The resistance of the
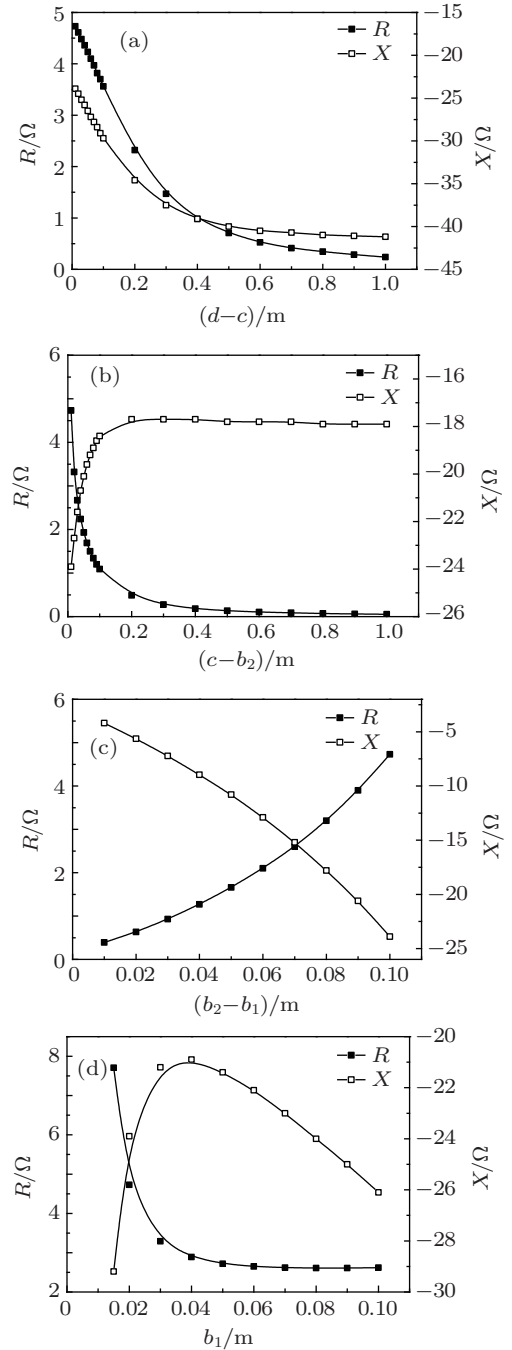
Fig. 3. (a) Antenna impedance versus distance $d - c$. $y_1 = 0.01$ m, $y_2 = 0.4$ m, $w = 0.1$ m, $b_1 = 0.02$ m, $b_2 - b_1 = 0.1$ m, $c - b_2 = 0.01$ m; (b) Antenna impedance versus distance $c - b_2$. $y_1 = 0.01$ m, $y_2 = 0.4$ m, $w = 0.1$ m, $b_1 = 0.02$ m, $b_2 - b_1 = 0.1$ m, $d - c = 0.01$ m; (c) Antenna impedance versus distance $b_2 - b_1$. $y_1 = 0.01$ m, $y_2 = 0.4$ m, $w = 0.1$ m, $b_1 = 0.02$ m, $c - b_2 = 0.01$ m, $d - c = 0.01$ m; (d) antenna impedance versus distance b_1. $y_1 = 0.01$ m, $y_2 = 0.4$ m, $w = 0.1$ m, $b_2 - b_1 = 0.1$ m, $c - b_2 = 0.01$ m, $d - c = 0.01$ m.

impedance $R = \mathrm{Re}(Z_A)$ and the reactance $X = \mathrm{Im}(Z_A)$ first fall down rapidly as $d - c$ increasing in Fig. 3(a). Then R and X remain almost unchanged as d–c increases beyond 60 cm. R in Fig. 3(b) is similar to that in Fig. 3(a) dependent on $c - b_2$ while X first increases with $c - b_2$ increasing. As shown in Fig. 3(c), R goes up and X falls down with the distance $b_2 - b_1$ increasing steadily. Figure 3(d) shows that R decreases with b_1 increasing rapidly and X reaches a maximum value at $b_1 = 0.04$ m approximately.

3.3. RF field structure

The three-dimensional (3D) distributions of the electric field $\left| E_y \right|$ in the poloidal and toroidal direction at the plasma edge are shown in Fig. 4 for a single strap ICRF antenna and for 4-strap ICRF antenna array in different toroidal phasing cases. We can see that the electric field with toroidal phasing $(0, \pi, 0, \pi)$ is much smaller than that with the phasing $(0, 0, 0, 0,)$.
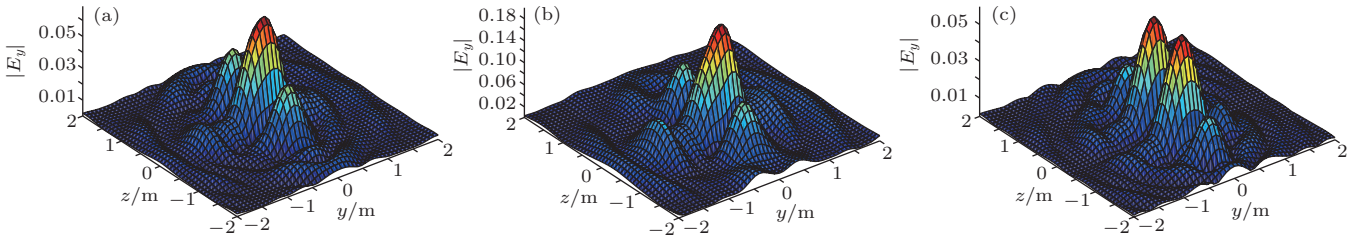

Fig. 4. (color online) (a) Distribution of $\left| E_y \right|$ at the plasma edge for the single antenna; (b) distribution of $\left| E_y \right|$ at the plasma edge for the 4-strap antenna array with toroidal phasing $(0, 0, 0, 0,)$ and period $\Delta z = 0.2$ m; (c) distribution of $\left| E_y \right|$ at the plasma edge for the 4-strap antenna array with toroidal phasing $(0, \pi, 0, \pi)$ and period $\Delta z = 0.2$ m; all with parameters: $y_1 = 0.01$ m, $y_2 = 0.4$ m, $w = 0.1$ m, $b_1 = 0.02$ m, $b_2 = 0.12$ m, $c = 0.13$ m, and $d = 0.14$ m.

4. Discussion and conclusions

A general variational formalism is used to evaluate the coupling of the ICRF antenna. The antenna resonant frequency is around 30 MHz in vacuum, and the presence of the plasma smooths the peak of the frequency response of the antenna resistance. The antenna resistance in the case of the plasma is much larger than the resistance with the vacuum condition due to the fact that the ICRF waves are absorbed in the plasma. The relationship between the impedance and the antenna parameters can be used to optimize the design of the ICRF antenna by maximizing the resistance R and minimizing the reactance X. The RF electric field distribution of the EAST 4-strap ICRF antenna shows that the antenna array with $(0, \pi, 0, \pi)$ phasing has lower electric field than with the $(0, 0, 0, 0)$ phasing. The mutual coupling between adjacent straps will be considered in the variational method in the future.

References

[1] Bhatnagar V P, Koch R, Messiaen A M and Weynants R R 1982 *Nucl. Fusion* **22** 280
[2] Koch R, Bhatnagar V P, Messiaen A M and Vaneester D 1986 *Comput. Phys. Commun.* **40** 1
[3] Mau T K, Chiu S C and Baker D R 1987 *IEEE Trans. Plasma Sci.* **15** 273
[4] Pecoul S, Heuraux S, Koch R and Leclert G 2002 *Comput. Phys. Commun.* **146** 166
[5] Theilhaber K and Jacquinot J 1984 *Nucl. Fusion* **24** 541
[6] Theilhaber K 1984 *Nucl. Fusion* **24** 1383
[7] Saigusa M, Yamamoto T, Petty C C, Yoshioka K, Kazumi H, Kawashima H, Fujii T, Kimura H, Miura Y and Tamai H 1993 *Nucl. Fusion* **33** 421
[8] Zhang X J, Qin C M and Zhao Y P 2005 *Chin. Phys.* **14** 2251